IEEE Access
Multidisciplinary ⋮ Rapid Review ⋮ Open Access Journal

Received 7 December 2023, accepted 4 January 2024, date of publication 15 January 2024, date of current version 24 January 2024.

Digital Object Identifier 10.1109/ACCESS.2024.3354163

RESEARCH ARTICLE

Design and Optimization of High Performance P3HT: PCBM Polymer Solar Cell Using P3HT Buffer Layer

AAQIB M. MIR[1], FAISAL BASHIR[2], (Member, IEEE), FAROOQ AHMAD KHANDAY[1], (Senior Member, IEEE), FURQAN ZAHOOR[3], (Member, IEEE), MEHWISH HANIF[4], AND ZAZILAH MAY[5], (Graduate Student Member, IEEE)

[1]Department of Electronics and IT, University of Kashmir, Srinagar 190006, India
[2]Department of Computer Engineering, College of Computer Science and Information Technology, King Faisal University, Hofuf 31982, Saudi Arabia
[3]Interdisciplinary Research Center for Advanced Materials, King Fahd University of Petroleum and Minerals, Dhahran 31261, Saudi Arabia
[4]Tyndall National Institute, University College Cork, Cork, T12R5CP Ireland
[5]Electrical and Electronics Engineering Department, Universiti Teknologi PETRONAS, Bandar Seri Iskandar, Perak 32610, Malaysia

Corresponding authors: Faisal Bashir (famed@kfu.edu.sa) and Zazilah May (zazilah@utp.edu.my)

This work was supported by Yayasan-Universiti Teknologi PETRONAS (YUTP-Fundamental Research Grant (FRG) 2021) under Grant 015LCO-327.

ABSTRACT In this paper, a novel structure of multilayer organic photovoltaic cell has been designed and simulated. The integration of Poly(3-hexylthiophene-2,5-diyl) (P3HT) buffer layer and Poly(9,9-bis(3'-(N,N-dimethyl) N- ethylammoinium propyl-2,7-fluorene)-alt-2,7-(9,9 dioctyl fluorene)) dibromide (PFN:BR) electron transport layer (ETL) in the proposed solar cell has improved the performance significantly. The various performance measuring parameters like power conversion efficiency (PCE), short circuit current (Jsc), open circuit voltage (Voc), fill factor (FF), quantum efficiency (QE) have improved significantly. Furthermore, the effect of different layer thickness, the density of traps N_t and temperature on the proposed solar cell has been studied and the optimum value has been obtained. It has been observed that after optimizing the different parameters of the proposed structure, the performance measuring parameters shows an improvement of 14%, 33.3%, 200% and 300% in Voc FF, Jsc and PCE respectively over the reported organic solar cells. Further, a QE of about 90% is achieved in the proposed structure.

INDEX TERMS Organic solar cell, energy harvesting, bulk heterojunction, buffer layer, power conversion efficiency, fill factor, quantum efficiency.

I. INTRODUCTION

These days, organic solar cell (OSC) technology drew much attention due to its design flexibility, lighter weight, low-cost manufacturing, swift increase in power conversion efficiency (PCE) and more importantly generation of clean and renewable energy. Nevertheless, shorter lifetimes of OSC, less efficiency as compared to inorganic solar cells and restricted environmental stability is proving as the major bottleneck in OSC marketing [1]. The low efficiency mainly arises because of the low diffusion length (∼few nanometres) and low carrier mobilities of organic materials [2]. In order to overcome these constraints, the bulk heterojunction (BHJ) concept has emerged as a favorable approach in organic solar cells (OSCs). This approach involves a slim mixture of conjugated polymers acting as electron donors and fullerene derivatives serving as electron acceptors, along with alternative methods that can be applied [3]. The able and widely used BHJ structure consists of poly (3- hexylthiophene) (P3HT) as electron donor material and phenyl- C61-butyric acid methyl ester (PCBM) as electron acceptor material. In this blend, the acceptor and donor materials create a lot of nano-interfaces, having a higher probability to reach the electrodes. The widely studied blend of P3HT:PCBM is greatly influenced

The associate editor coordinating the review of this manuscript and approving it for publication was Adamu Murtala Zungeru.

by the phase morphology of the Donor/Acceptor interface. Morphology has a great influence on the light absorption, dissociation and transport of charges and generation and recombination of charges [4], [5]. Various techniques have been introduced to shape the active layer morphology. And one of the encouraging techniques is the buffer layer insertion in the conventional OSC structure. The buffer layer significantly increases the charge generation and reduces the recombination at the hole transport layer (HTL)/BHJ interface. The buffer layer not only works as an HTL layer but also enhances the photon absorption of the device [6]. Besides, the OSCs based on P3HT: PCBM morphology have demonstrated power conversion efficiency of 4% to 5% [7], [8]. However, with the use of low bandgap materials, the power conversion efficiency has surpassed the mark of 10% [9], [10]. With a single BHJ, it reached up to 17.1%, as reported by Lin et al. [11]. Recently, non-fullerene (NF) acceptor-based BHJ OSC was fabricated by Liu et al. [12] with a PCE of 18.22%, which has the highest record of PCE to date for a single junction BHJ OSC device. However, the achievement of environmental stability of OSC and its longer lifetime still poses a challenge, researchers are looking to overcome. The oxidation of PCBM, due to the dispersal of oxygen and other atmospheric gases into the P3HT: PCBM active layer, serves as the main reason for the degradation in the absorption and exciton generation of the structure [13], [14].

Although few number of devices of the P3HT: PCBM OSC have been fabricated with P3HT buffer layer. Here in this particular study, we are introducing the first simulated P3HT: PCBM cell with P3HT as the buffer layer. We have investigated the impact of various technological and material parameters on the performance of the proposed device and have optimized these parameters to enhance its efficiency. While optimizing these parameters, the range of the material properties as available in the literature has been strictly followed. Device simulation is a great appliance to examine the characteristics of the device and optimize the material properties to enhance efficiency. Researchers have effectively employed the solar cell capacitance simulator (SCAPS) to simulate a variety of solar cells, including OSCs, cadmium telluride (CD-Te), copper indium gallium selenide (CIGS), and perovskite cells, among others [15], [16].

In this work, the SCAPS software has been utilized for the purpose of device simulation of P3HT: PCBM solar cell. Several parameters have been studied that affect the performance of the blend. In the first place, the effect of variation of the active layer thickness on the performance parameters of the cell was considered thoroughly. Next, the impact of the insertion of the P3HT buffer layer on current-voltage characteristics (IV) was taken into account and it was observed that the open-circuit voltage (V_{OC}) increases by 7%. PCE enhances by 17.3% with the incorporation of a buffer layer. The effect of change of technological parameters of electron transport and hole transport layers was also studied. Furthermore, the impact of the change of defect densities of various layers on IV curve and PCE was taken into account. Finally,

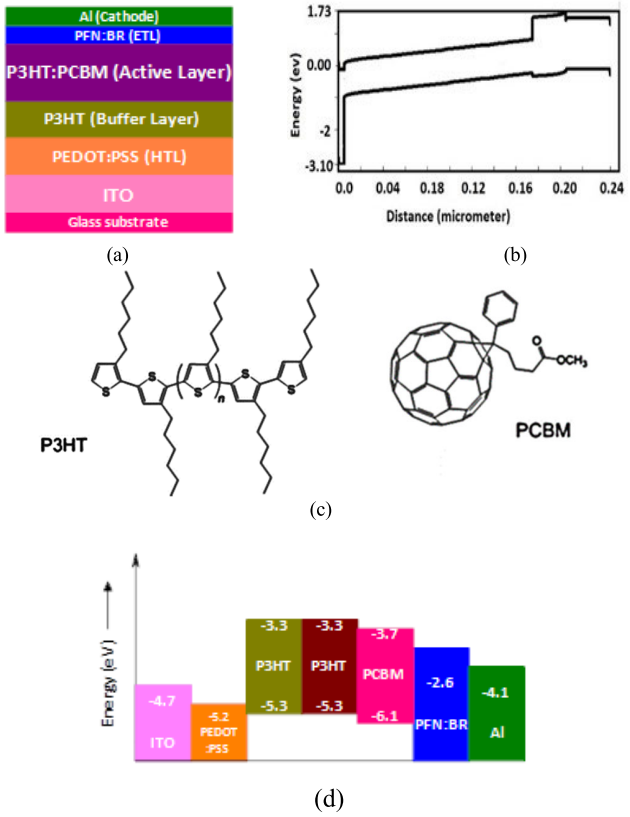

FIGURE 1. Proposed multi-layer organic solar cell (a) schematics (b) Band diagram after contact (c) Molecular structure of P3HT and PCBM (d) Band position before contact.

the impact of temperature variations is studied for realizing the enhancement in PCE. By optimizing the properties of active, buffer, ETL and HTL layers, the PCE has been enhanced to a significant extent with respect to the reported OSCs (Table 2).

II. MODELS AND METHODS

SCAPS version (3.3.10) have been utilized for the simulation of the proposed OSC structure. SCAPS, a windows-oriented solar cell simulation program is a one dimensional tool. It is designed by the Department of Electronics and Information Systems (ELIS), University of Gent, Belgium. The software uses three recombination mechanisms viz direct band to band, Auger and SRH. By solving equations such as Poisson's equation and the continuity equation for electrons and holes, the solar cell capacitance simulator (SCAPS) is capable of simulating both the electrical and optical characteristics of a solar cell. The multilayer structure of the proposed organic solar cell (OSC) comprises of Glass substrate/ITO/PEDOT:PSS/P3HT/P3HT:PCBM/PFN:BR/Al. ITO (Indium tin oxide) and Al (Aluminium) operate as front contact (anode) and back contact (cathode) respectively as shown in Fig.1. PFN:BR forms the electron transport layer (ETL) and PEDOT: PSS acts as HTL. P3HT functions as the buffer layer in the presented structure. Fig.1 (b) and (d) display the energy band alignment of the structure after the

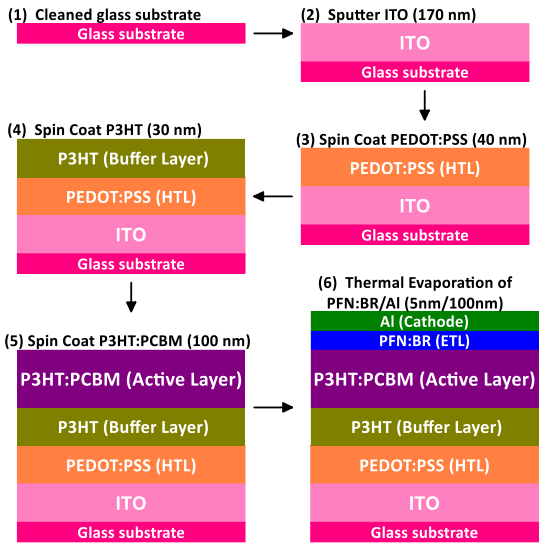

FIGURE 2. Proposed fabrication flow of the multi-layer OSC.

contact and before the contact respectively. The molecular structure of P3HT and PCBM is presented in Fig. 1 (c). [9]

The fabrication steps for the proposed multilayer OSC are shown in Fig. 2. The fabrication steps start with the glass slide, which is cleaned using Decon-90 to remove dust, metallic and other non-metallic contaminations. Subsequently, the slides need to be soaked in acetone, then a layer of ITO be deposited by the process of sputtering onto the cleaned glass slides. The ITO patterned with glass slides, be exposed to O_2 plasma treatment. The thickness monitor can be used to monitor the thickness. Subsequently, ITO coated with glass samples be annealed at high temperatures before the deposition of the PEDOT:PSS layer. The PEDOT:PSS be ultra-sonicated and spin coated, before its deposition on glass coated ITO layer. The next step is the preparation of the P3HT buffer layer solution in chlorobenzene and spin coat it on PEDOT:PSS. The active layer P3HT:PCBM blend, need to be prepared in the ratio of 1:1. P3HT:PCBM layer should be then spin coated on the buffer layer and be annealed at different temperatures [6]. Finally, thermal vacuum evaporation be utilized to deposit ETL (PFN:BR) layer and Al cathode samples [17].

III. DEVICE SIMULATION PARAMETERS

Table 1 displays the technical parameters utilized during the course of simulation. In this table, E_g, ε_r and χ represent the bandgap, relative permittivity and electron affinity respective

In the given context, the symbols μ_n and μ_p represent the mobility of electrons and holes, respectively. Meanwhile, N_c and N_v indicate the effective density of states for the conduction and valence bands, respectively. N_A and N_D represent donor and acceptor concentrations respectively, whereas N_t act for defect density. The defects can be introduced in the active layer as well at the interfaces. The defect density at the interfaces including ETL/Active, Active/Buffer Layer, and Buffer Layer/HTL are taken to be $1\times10^{9}\text{cm}^{-2}$. The value of $1.5\times10^{-18}\text{cm}^{2}$ is taken to be the capture cross section of electrons and holes [18] for all the layers. Thermal velocity for both electrons and holes is considered to be as 10^{7}cm/s. Moreover the energy level of the traps is considered as neutral with position at 0.04 eV [18] with regard to the centre of the bandgap, E_g. The work function of the back and front contact is taken to be 4.1 eV and 4.7 eV respectively. The ε_r, of the active layer is computed by taking the average of the relative permittivity of donor and acceptor materials as reported in the reference [19]. The bandgap of the active layer is calculated by taking difference between LUMO of acceptor (PCBM) and HOMO of donor material (P3HT) as reported in the reference [18].

The bandgap of the active layer is calculated by taking difference between LUMO of acceptor (PCBM) and HOMO of donor material (P3HT) as reported in the reference [16].

For the source of light, Air Mass Global (AM 1.5 G), having an integrated power of 1000 watt/m2 is considered. In this simulation, no optical reflectance is being considered.

The absorption modal of P3HT:PCBM is taken from the absorption profile reported in the reference [19] and the absorption modal of P3HT is taken from the reported work [20].

TABLE 1. Technical and physical parameters used in the simulation.

Parameters	HTL [24]	BL [18]	AL [19]	ETL [24]
Thickness (nm)	40	30 [23]	100 [24]	5
E_g	1.6	1.85	1.05[18]	2.98
ε_r (relative)	3	3.4	3.8	5
χ (ev)	3.4	3.1	3.8	4
$\mu_n\,(cm^2v^{-1}s^{-1})$	4.5×10^{-4}	1×10^{-4}	2×10^{-3}	1×10^{-6}
$\mu_p(cm^2v^{-1}s^{-1})$	9.9×10^{-5}	1×10^{-3}	2×10^{-3}	1×10^{-4}
$N_A(cm^{-3})$	2×10^{-4}	0	0	9×10^{20}
$N_D(cm^{-3})$	0	3.17×10^{13}	0	0
$N_c(cm^{-3})$	1×10^{22}	1×10^{22}	7.8×10^{22}	1×10^{19}
$N_v(cm^{-3})$	1×10^{22}	1×10^{22}	7.8×10^{19}	1×10^{19}

We calibrated our model parameters with the experimental data as listed in Table 1 to obtain the characteristics reported in [22] as shown in Fig. 3. In Fig. 3, the simulation outcomes indicate a high degree of concordance with the experimental results.

The IV (current-voltage) characteristics of the proposed solar cell structure are demonstrated in Fig. 4, both under illuminated and dark conditions. Both the I-V curves are plotted at 170 nm active layer(P3HT:PCBM) thickness. The dark characteristics presented in Fig. 4(a) is extrapolated to find the values of reverse saturation current density (J_o), series resistance (R_s), shunt resistance (R_{sh}) and ideality factor (n). The extrapolated straight line portion of the log I-V curve and

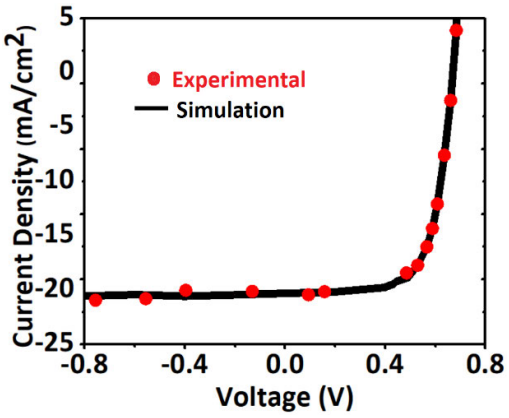

FIGURE 3. Calibration against the work done using experimental data as conveyed in [22].

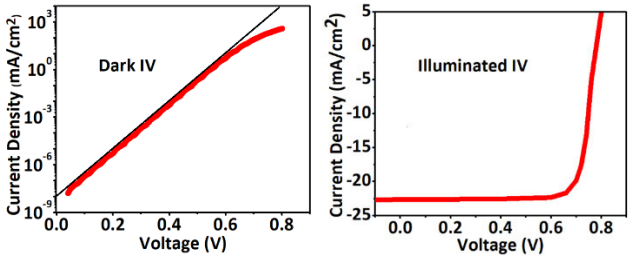

FIGURE 4. a) Dark I-V curve of the proposed structure b) Illuminated I-V curve of the proposed structure.

the current axis at V=0, intersection, gives the value of the reverse saturation current density.

From Fig.4(a), we have, $J_o = 1.62 \times 10^{-8}$mA/cm^2. By calculating the inverse of slope of dark IV curve at V_{oc} and the inverse of slope at condition V=0 respectively, the series and shunt resistance are determined. Accordingly, the values of R_s and R_{sh} are calculated as 0.3 Ω and 144.7 KΩ respectively. The slope of the linear portion of the semi log dark I-V curve results in the ideality factor, n =1.5. The lower values of R_s and n reflect the higher values of Fill Factor (FF) and good material quality respectively. The impact of different parameters on the output of the cell is investigated to optimize the proposed structure's performance measurement parameters.

IV. THE EFFECT OF TECHNOLOGICAL PARAMETERS ON THE PERFORMANCE OF SOLAR CELL

The parameters studied include the thickness of the active layer, the presence of a buffer layer, the density of traps N_t, the mobility of electrons and holes, the electron affinity, and the effect of temperature variation.

A. EFFECT OF ACTIVE LAYER THICKNESS

To examine its impact on the performance of the OSC structure, the thickness of the active layer has been adjusted from 100 nm to 400 nm. The efficiency of the BHJ OSC is a product function and mainly depend on four processes, which are photon absorption and exciton creation, diffusion

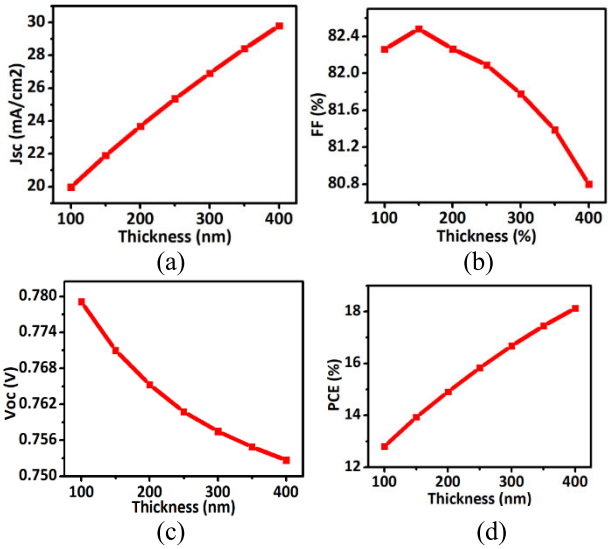

FIGURE 5. Effect of the active layer thickness variation on (a) Jsc (b) FF (c) Voc (d) PCE.

of exciton, charge transfer and the charge collection. All these processes form a strong function of the active layer (P3HT:PCBM) thickness. As per the Beer Lambert's law, the absorption varies linearly with the active layer thickness. Increased thickness corresponds to the increased number of absorbed photons. Because of the enhanced absorption of photons with the increased thickness, the short circuit current (J_{sc}) and power conversion efficiency (PCE), increase as shown in Fig. 5(a) and 5(d) respectively. At the optimum thickness of 170 nm, the J_{sc} and the PCE reach the value of 22.6 mA/cm^2 and 14.32 % respectively. Both these output parameters increase slightly beyond this thickness. Nevertheless, the increase in absorption comes at the cost of increase in recombination of free charge carriers in the active layer, as can be understood from equation 1.

$$E_{int} = \frac{V_{oc} V_{app}}{\tau} \tag{1}$$

where E_{int} is the internal electric field, V_{oc}&V_{app} are open circuit voltage and the applied voltage. τ represents the active layer thickness in equation (1). The increase in the thickness causes the electric field to get reduced, consequently reducing the carrier transport length, which indirectly increases the recombination phenomenon. Equation (2) demonstrates that the V_{oc} is influenced by both the dark generation and saturation currents [24].

$$V_{oc=\frac{nKT}{q}} \ln\left(\frac{I_l}{I_o} - 1\right) \tag{2}$$

The reverse saturation current decreases as the thickness increases which in turn decreases the V_{oc} as shown in Fig. 5(c).

The drop in the V_{oc} minimises as the thickness increases to higher values. The FF with respect to the thickness has been plotted in Fig. 5(b). The sharp decrease in the FF from 82.26% to 82.09% is due to the increase in the series resistance with increase in the layer thickness.

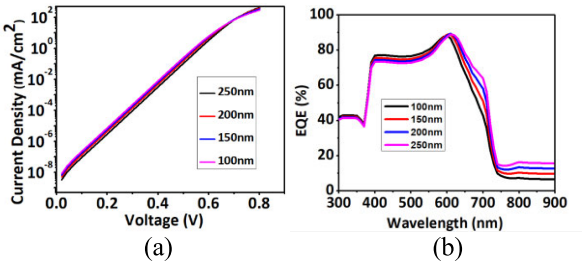

FIGURE 6. Effect of the variation of the active layer thickness on (a) dark current density (b) EQE.

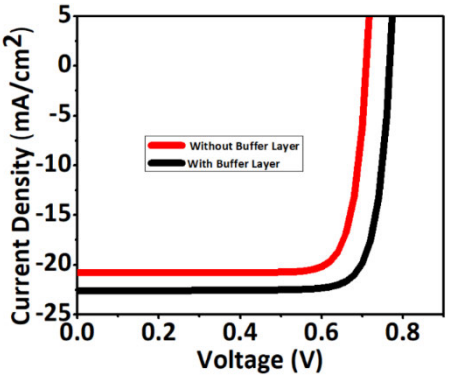

FIGURE 7. The illuminated I-V curve with and without buffer layer.

The dark I-V curve at different thickness from 100 nm to 250 nm has been plotted in Fig. 6(a). Furthermore, the external quantum efficiency (EQE) at different values of thickness has been plotted in Fig. 6(b). The results from Fig. 6(b) testify that the EQE increases with increase in the thickness of the active layer. This enhancement is again due to the increase in the absorption of the light. However, EQE show a slight decrease in the range between 400 nm to 600 nm wavelength. The decrease is because of the increase in the recombination effects at high values of thickness. In order to balance the absorption of light and the recombination of charges, the thickness of the active layer has been selected as 170 nm.

B. EFFECT OF INSERTION OF BUFFER LAYER

The light I-V curve with and without buffer layer is shown in Fig. 7. With the insertion of buffer layer between HTL layer and the active layer, the J_{sc} of the device increases from 20.7 mA/cm^2 to 22.63 mA/cm^2 and similar trend is being observed in PCE. The PCE of the proposed structure with buffer layer, has been observed as 14.32% whereas without the buffer layer, it is 12.20%. Hence PCE shows an improvement of 17.3% by the incorporation of buffer layer. Furthermore the consequence of the buffer layer thickness on PCE is shown in Fig. 8(a). The thickness of the buffer layer has been varied from 20nm to 50nm and the PCE increases from 14.32% to 14.45% respectively.

By inserting the buffer layer, V_{oc} of the device slightly increased from 0.71 V to 0.76 V. The FF of both the structures is almost identical. The enhancement in the PCE is primarily dominated by the rise in J_{sc}. This is because of the reason that incorporation of the buffer layer enhances the absorption as

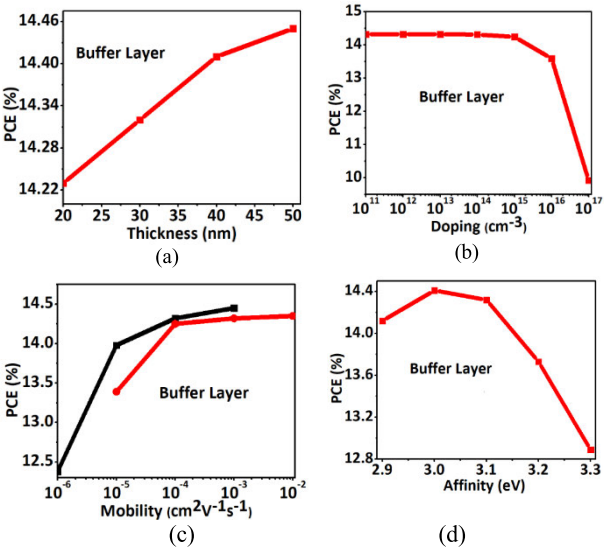

FIGURE 8. Change of the PCE with the (a) thickness of buffer layer (b) doping concentration of buffer layer (c) electron and hole mobility of the buffer layer (d) electron affinity of the buffer layer.

well as minimizes the recombination losses by offering the unrestricted transport of holes to the anode [6]. The enhancement in the PCE accords with the increase in the absorption. However FF shows a decrease from 83.01% to 81.31%. As a result, the optimal thickness of the buffer is set to be 30nm.

Additionally, the effect of the doping concentrations N_D on the PCE is displayed in Fig 8(b). The doping concentration is varied from 10^{11} cm^{-3} to 10^{17} cm^{-3}. The PCE is saturated at 14.32 % from10^{11} cm^{-3} to 10^{13} cm^{-3} and it shows a decline from 10^{14} cm^{-3}. The decrease in the PCE is due to decrease in J_{sc}. Fig. 8(c) shows the impact of electron and hole mobility on the PCE of the device. The electron mobility was changed from 10^{-6} cm^{2}V^{-1}s^{-1} and hole mobility was altered from 10^{-5} cm^{2}V^{-1}s^{-1} to 10^{-3} cm^{2}V^{-1}s^{-1}. The highest PCE of 14.45% was achieved at electron mobility of 10^{-3} cm^{2}V^{-1}s^{-1} and PCE of 14.35% was simulated at hole mobility of 10^{-2}.

The stability of the OSC greatly depends on the electron affinity as suggested in [25]. Fig. 8(d) shows the variation of electron affinity of the buffer layer on the PCE. The electron affinity is changed from 2.9 eV to 3.3 eV. The PCE first increases and after reaching the value of 14.32% at an optimal electron affinity value of 3.1 eV, a decline is observed in the value of PCE.

C. EFFECT OF CHANGE OF DEFECT DENSITY

The relationship between the defect density N_t and the lifetime τ and diffusion length L of the charge carriers can be explained through the following equations [26],

$$\tau = \frac{1}{\sigma . N_t . V_{th}} \tag{3}$$

$$L = \sqrt{D\tau} \tag{4}$$

where σ represents the capture cross section of the minority carriers, V_{th} symbolizes the thermal velocity and D is the

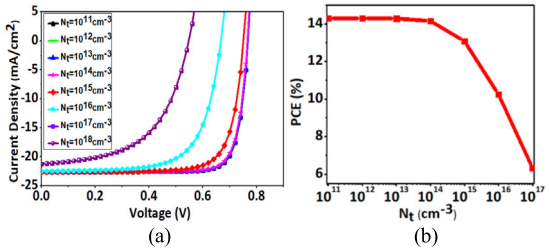

FIGURE 9. Influence of the change of the defect density, N_t of the active layer on (a) I-V characteristics (b) PCE.

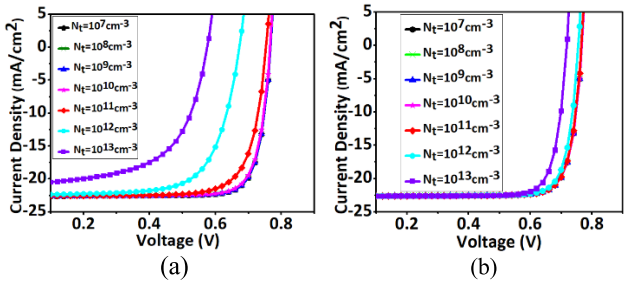

FIGURE 10. The impact of the defect densities of (a) Active/Buffer interface (b) ETL/Active interface, on the I-V characteristics.

diffusion constant. The equation (3) and (4) illustrates that as the defect density upsurges, the carrier lifetime and the diffusion length decreases. The effect of the defect density on the I-V characteristics is shown in Fig. 9(a). The curves specify that as the N_t increases the cell performance characteristics degrades because of the decrease in the carrier life time τ, which leads to increase in the recombination rate. As indicated in Fig. 9(b), as the defect density increases from 10^{12} cm^{-3} to 10^{13} cm^3, the PCE drop's from 14.29 % to 14.28%. The drop is more evident when N_t equals 10^{15} cm^{-3} and PCE is 13.07 %. Hence defect density value is calibrated at10^{12} cm^{-3}.

The effect of defect densities at the interfaces has also been studied. In our proposed structure we define three interfaces namely ETL/Active, Active/Buffer and Buffer/HTL interfaces. In all the three interfaces the defect densities has been changed from 10^7 cm^{-3} to 10^{13} cm^{-3}.

The effect of defect densities at buffer/active interface on I-V characteristics is shown in Fig. 10(a). As can be seen from the Fig 10 itself that as N_t increases, the cell performance decreases because of the hike in the charge recombination. When N_t of P3HT:PCBM/P3HT interface equals 10^7 cm^{-3}, the PCE shows a value of 14.32%. As N_t reaches the value of 10^9 cm^{-3}, the PCE drops to 14.30%. It further degrades as the value of N_t increases. Fig. 10(b) displays the impact of the variation of the defect density of the ETL/active interface on the IV characteristics. In comparison to the buffer/active interface, the degradation in the performance is lower in ETL/active interface. From 10^7 cm^{-3} to 10^9 cm^{-3} value of N_t, the PCE shows a constant value of 14.30% and decreases to 14.29% at N_t of 10^{10} cm^{-3}.

Also the active/HTL interface defects do not show any major influence on the cell performance. So, as the defect density at the interfaces is increased, more traps are generated leading to more recombination of charges. Hence, 10^7 cm^{-3} is taken as the optimised value of the N_t at the interfaces.

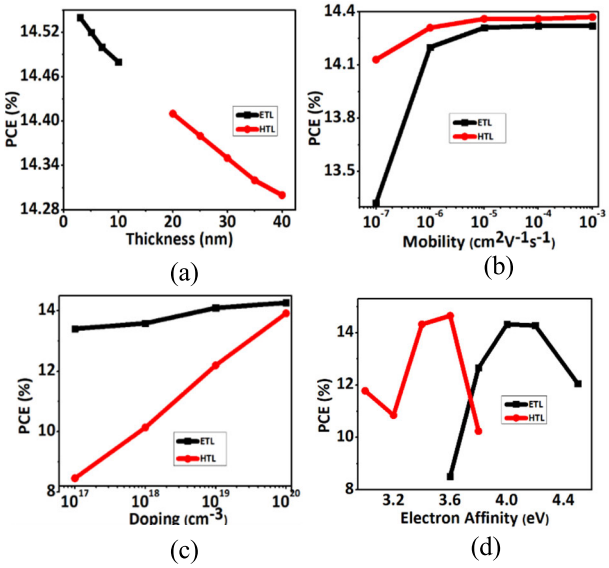

FIGURE 11. Effect of change of technological parameters of ETL and HTL layers on PCE (a) Thickness (b) Mobility (c) Doping (d) Electron Affinity.

D. EFFECT OF ETL AND HTL CHARACTERISTICS

The transporting layers, that is, ETL and HTL layers act as the exciton blocking layers and has the great importance to enhance the charge collection property of the device. Polymer such as PEDOT:PSS and conjugated electrolyte polymer like PFN:BR are widely used as HTL and ETL layers in OSC respectively. Several efforts have been made to enhance the properties for instance mobility, electron affinity and doping of the transporting layers [27], [28]. By analyzing the effects of changes in thickness, electron affinity, mobility, and doping of the transporting layers, we evaluated how these properties impact the PCE of the simulated structure. Fig. 11(a) shows the effect of the change of the thickness of the ETL and HTL layers on the PCE. The thickness of the ETL has been varied from 3 nm to 10 nm and the doping of the HTL layer has been changed from 20 nm to 40 nm. In both the cases increased thickness reduces the PCE of the device due to increase in the series resistance. The highest PCE of 14.54 % has been achieved for ETL thickness of 3 nm. For HTL thickness of 20 nm PCE reaches up to 14.41%. The effect of the mobility of ETL and HTL on PCE has been demonstrated in Fig. 11(b). The electron mobility and hole mobility of the ETL and HTL layers respectively, has been changed from 10^{-7} cm^{2}V^{-1}s^{-1} to 10^{-3} cm^{2}V^{-1}s^{-1}. The increase in the mobility increases the conductivity and consequently reduces the series resistance. The maximum PCE of 14.32% is achieved at HTL hole mobility of 10^{-3} cm^{2}V^{-1}s^{-1} and at the same value of ETL electron mobility, the PCE reaches up to the value of 14.37%.

Moreover, the doping concentration N_D and N_A of ETL and HTL layers respectively, has been changed from 10^{17} cm^{-3}

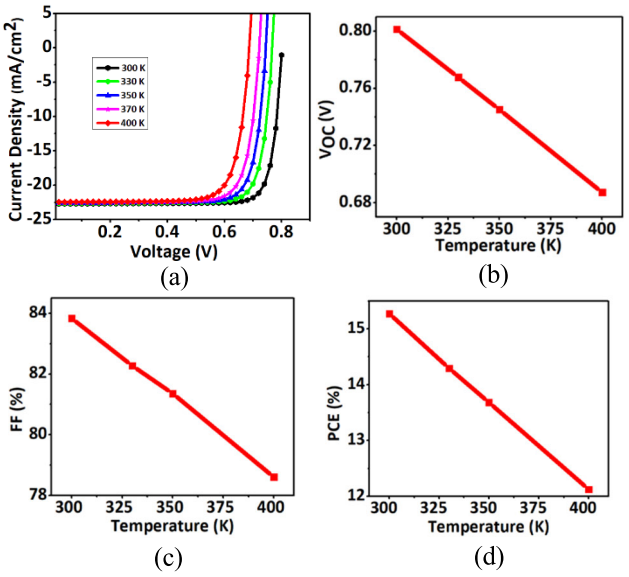

FIGURE 12. The impact of the variation of temperature on (a) IV curve (b) V_{OC} (c) FF (d) PCE.

TABLE 2. Photovoltaic properties of different OSC devices reported in the literature.

Ref.	V_{oc} (V)	J_{sc} (mA/cm^2)	FF (%)	PCE (%)
[29]	0.59	15.21	45.50	4.07
[30]	0.58	18.65	55.88	6.03
[31]	0.55	19.8	50	5.3
[23]	0.72	19	63	8.62
[32]	0.60	16.31	76.6	7.61
[22]	0.66	12.01	59	4.65
This Work	**0.76**	**22.6**	**82.33**	**14.32**

to 10^{20} cm^{-3}. Fig. 11(c) shows the results of the simulation. A positive development in the PCE is observed by increasing the doping concentration. At doping value of 10^{20} cm^{-3}, the PCE shows the maximum value of 13.92% and 14.72% for HTL and ETL layers respectively.

Furthermore, the impact of the variation of the electron affinity of the ETL and HTL layers has been displayed in Fig. 11(d). The electron affinity of the ETL layer has been changed from 3.6 eV to 4.5 eV. The maximum PCE of 14.32 % has been attained for the electron affinity of 4eV. In addition, the affinity of the HTL has been changed from 3eV to 3.8eV and the maximum PCE of 14.65% has been acquired at electron affinity of 3.6eV.

E. EFFECT OF VARIATION OF WORKING TEMPERATURE

The impact of the change in working temperature on different cell parameters have been studied. Organic solar cells are considered very sensitive towards temperature changes. The temperature was changed between 300 K and 400 K. Fig. 12(a) shows the effect of the variation of temperature on the I-V curve of the device. As the temperature increases, the Voc of the device shows a significant drop from 0.8 V to 0.62 V. This decrease in Voc is because of the hike in the reverse saturation current and the recombination of the charges. The effect of temperature on Voc can be more clearly visualized from Fig.12 (b). Also, the FF and PCE decreases linearly in a similar fashion as that of Voc as shown in Figs. 12(c) and 12(d) respectively. The short circuit current shows a constant value with respect to the variation of the temperature from 300 K to 400 K.

Table 2 shows the performance comparison of the proposed Multi-Layer OSC with the state of the art organic solar cell presented in the literature.

V. CONCLUSION

This work conducted a comprehensive analysis of a simulated organic solar cell structure comprising glass/ITO/PEDOT:PSS/P3HT/P3HT:PCBM/PFN:BR/Al, aiming to optimize key performance metrics crucial for enhancing solar cell efficiency. The study targeted key parameters PCE, Jsc, Voc, FF, and QE, known to pose challenges in P3HT:PCBM organic solar cell. Through strategic integration of a P3HT buffer layer and meticulous device optimization, substantial improvements were observed. Notably, there was a significant enhancement of 14% in Voc, 33.3% in FF, 200% in Jsc, and an impressive 300% in PCE over previously reported organic solar cells.

REFERENCES

[1] D. J. Lipomi, H. Chong, M. Vosgueritchian, J. Mei, and Z. Bao, "Toward mechanically robust and intrinsically stretchable organic solar cells: Evolution of photovoltaic properties with tensile strain," *Sol. Energy Mater. Sol. Cells*, vol. 107, pp. 355–365, Dec. 2012.

[2] S. M. Menke and R. J. Holmes, "Exciton diffusion in organic photovoltaic cells," *Energy Environ. Sci.*, vol. 7, no. 2, pp. 499–512, 2014.

[3] A. K. Dikshit, S. Maity, N. Mukherjee, and P. Chakrabarti, "Hybrid inorganic–organic inverted solar cells with ZnO/ZnMgO barrier layer and effective organic active layer for low leakage current, enhanced efficiency, and reliability," *IEEE J. Photovolt.*, vol. 11, no. 4, pp. 983–990, Jul. 2021, doi: 10.1109/JPHOTOV.2021.3067828.

[4] B. Ray, P. R. Nair, and M. A. Alam, "Annealing dependent performance of organic bulk-heterojunction solar cells: A theoretical perspective," *Sol. Energy Mater. Sol. Cells*, vol. 95, no. 12, pp. 3287–3294, Dec. 2011, doi: 10.1016/j.solmat.2011.07.006.

[5] W. Ma, C. Yang, X. Gong, K. Lee, and A. J. Heeger, "Thermally stable, efficient polymer solar cells with nanoscale control of the interpenetrating network morphology," *Adv. Funct. Mater.*, vol. 15, no. 10, pp. 1617–1622, Oct. 2005, doi: 10.1002/adfm.200500211.

[6] I. C. Ghosekar and G. C. Patil, "Performance analysis and thermal reliability study of multilayer organic solar cells," *IEEE Trans. Device Mater. Rel.*, vol. 19, no. 3, pp. 572–580, Sep. 2019, doi: 10.1109/TDMR.2019.2933312.

[7] G. Yu, J. Gao, J. C. Hummelen, F. Wudl, and A. J. Heeger, "Polymer photovoltaic cells: Enhanced efficiencies via a network of internal donor-acceptor heterojunctions," *Science*, vol. 270, pp. 1789–1791, Dec. 1995.

[8] J. J. M. Halls, C. A. Walsh, N. C. Greenham, E. A. Marseglia, R. H. Friend, S. C. Moratti, and A. B. Holmes, "Efficient photodiodes from interpenetrating polymer networks," *Nature*, vol. 376, no. 6540, pp. 498–500, Aug. 1995.

[9] L. Liirò-Peluso, J. Wrigley, D. B. Amabilino, and P. H. Beton, "Submolecular resolution imaging of P3HT:PCBM nanostructured films by atomic force microscopy: Implications for organic solar cells," *ACS Appl. Nano Mater.*, vol. 5, no. 10, pp. 13794–13804, Oct. 2022, doi: 10.1021/acsanm.2c01399.

[10] I. Etxebarria, J. Ajuria, and R. Pacios, "Solution-processable polymeric solar cells: A review on materials, strategies and cell architectures to overcome 10%," *Organic Electron.*, vol. 19, pp. 34–60, Apr. 2015.

[11] Y. Lin, Y. Firdaus, M. I. Nugraha, F. Liu, S. Karuthedath, A. Emwas, W. Zhang, A. Seitkhan, M. Neophytou, H. Faber, E. Yengel, I. McCulloch, L. Tsetseris, F. Laquai, and T. D. Anthopoulos, "17.1% efficient single-junction organic solar cells enabled by n-type doping of the bulk-heterojunction," *Adv. Sci.*, vol. 7, no. 7, Apr. 2020, Art. no. 1903419, doi: 10.1002/advs.201903419.

[12] Q. Liu, Y. Jiang, K. Jin, J. Qin, J. Xu, W. Li, J. Xiong, J. Liu, Z. Xiao, K. Sun, S. Yang, X. Zhang, and L. Ding, "18% efficiency organic solar cells," *Sci. Bull.*, vol. 65, no. 4, pp. 272–275, 2020.

[13] N. Chander, E. Jayaraman, M. Rawat, A. Bagui, and S. S. K. Iyer, "Stability and reliability of PTB7:PC71BM and PTB7:PC61BM inverted organic solar cells: A comparative study," *IEEE J. Photovolt.*, vol. 9, no. 1, pp. 183–193, Jan. 2019.

[14] A. Perthué, T. Gorisse, H. S. Silva, C. Lombard, D. Bégué, P. Hudhomme, B. Pépin-Donat, A. Rivaton, and G. Wantz, "New insights into polymer solar cells stability: The crucial role of PCBM oxidation," *J. Mater. Res.*, vol. 33, no. 13, pp. 1868–1878, Jul. 2018.

[15] S. Baruah, J. Borah, S. Bhattarai, and S. Maity, "Optimization of all inorganic perovskite solar cell with dual active layers for beyond 29% efficiency," *Sol. Energy*, vol. 263, Oct. 2023, Art. no. 111939.

[16] M. Burgelman, P. Nollet, and S. Degrave, "Modelling polycrystalline semiconductor solar cells," *Thin Solid Films*, vols. 361–362, pp. 527–532, Feb. 2000.

[17] I. C. Ghosekar and G. C. Patil, "Improving organic solar cell efficiency using solution processed poly (3-hexylthiophene) buffer layer," *Micro Nano Lett.*, vol. 14, no. 1, pp. 74–77, Jan. 2019, doi: 10.1049/mnl.2018.5178.

[18] Z. Bahrami, A. Salehi, and A. M. Eyvaraghi, "AMPS-1D modelling of P3HT/PCBM bilayer and BHJ organic solar cell," in *Proc. 27th Iranian Conf. Electr. Eng. (ICEE)*, Apr. 2019, pp. 41–45, doi: 10.1109/IranianCEE.2019.8786641.

[19] T. J. K. Brenner, I. Hwang, N. C. Greenham, and C. R. McNeill, "Device physics of inverted all-polymer solar cells," *J. Appl. Phys.*, vol. 107, no. 11, Jun. 2010, Art. no. 114501, doi: 10.1063/1.3371364.

[20] J. Müllerová, M. Kaiser, V. Nádaždy, P. Siffalovic, and E. Majková, "Optical absorption study of P3HT:PCBM blend photo-oxidation for bulk heterojunction solar cells," *Sol. Energy*, vol. 134, pp. 294–301, Sep. 2016.

[21] S. Miller, G. Fanchini, Y.-Y. Lin, C. Li, C.-W. Chen, W.-F. Su, and M. Chhowalla, "Investigation of nanoscale morphological changes in organic photovoltaics during solvent vapor annealing," *J. Mater. Chem.*, vol. 18, no. 3, pp. 306–312, 2008, doi: 10.1039/B713926H.

[22] M. Shaban, M. Benghanem, A. Almohammedi, and M. Rabia, "Optimization of the active layer P3HT:PCBM for organic solar cell," *Coatings*, vol. 11, no. 7, p. 863, Jul. 2021, doi: 10.3390/coatings11070863.

[23] B. M. Omer, A. Khogali, and A. Pivrikas, "AMPS-1D modeling of P3HT/PCBM bulk-heterojunction solar cell," in *Proc. 37th IEEE Photovoltaic Specialists Conf.*, Jun. 2011, pp. 734–743, doi: 10.1109/PVSC.2011.6186059.

[24] W. Abdelaziz, A. Shaker, M. Abouelatta, and A. Zekry, "Possible efficiency boosting of non-fullerene acceptor solar cell using device simulation," *Opt. Mater.*, vol. 91, pp. 239–245, May 2019, doi: 10.1016/j.optmat.2019.03.023.

[25] E. T. Hoke, I. T. Sachs-Quintana, M. T. Lloyd, I. Kauvar, W. R. Mateker, A. M. Nardes, C. H. Peters, N. Kopidakis, and M. D. McGehee, "The role of electron affinity in determining whether fullerenes catalyze or inhibit photooxidation of polymers for solar cells," *Adv. Energy Mater.*, vol. 2, no. 11, pp. 1351–1357, Nov. 2012.

[26] D. Yeboah and J. Singh, "Dependence of exciton diffusion length and diffusion coefficient on photophysical parameters in bulk heterojunction organic solar cells," *J. Electron. Mater.*, vol. 46, no. 11, pp. 6451–6460, Nov. 2017, doi: 10.1007/s11664-017-5679-2.

[27] H. Frohne, D. C. Müller, and K. Meerholz, "Continuously variable hole injection in organic light emitting diodes," *Chem. Phys. Chem.*, vol. 3, no. 8, pp. 707–711, 2002, doi: 10.1002/1439-7641(20020816)3:8<707::AID-CPHC707>3.0.CO;2-3.

[28] H. Shi, C. Liu, Q. Jiang, and J. Xu, "Effective approaches to improve the electrical conductivity of PEDOT:PSS: A review," *Adv. Electron. Mater.*, vol. 1, no. 4, Apr. 2015, Art. no. 1500017, doi: 10.1002/aelm.201500017.

[29] M. S. Hamed and G. T. Mola, "Copper sulphide as a mechanism to improve energy harvesting in thin film solar cells," *J. Alloys Compounds*, vol. 802, pp. 252–258, Sep. 2019, doi: 10.1016/j.jallcom.2019.06.108.

[30] M. S. G. Hamed, S. O. Oseni, A. Kumar, G. Sharma, and G. T. Mola, "Nickel sulphide nano-composite assisted hole transport in thin film polymer solar cells," *Sol. Energy*, vol. 195, pp. 310–317, Jan. 2020, doi: 10.1016/j.solener.2019.11.068.

[31] X. G. Mbuyise and G. T. Mola, "Polycrystal metals nano-composite assisted photons harvesting in thin film organic solar cell," *Sol. Energy*, vol. 208, pp. 930–936, Sep. 2020, doi: 10.1016/j.solener.2020.08.048.

[32] M. Omrani, H. Fallah, K.-L. Choy, and M. Abdi-Jalebi, "Impact of hybrid plasmonic nanoparticles on the charge carrier mobility of P3HT:PCBM polymer solar cells," *Sci. Rep.*, vol. 11, no. 1, p. 19774, Oct. 2021.

AAQIB M. MIR was born in Jammu and Kashmir, India, in 1998. He received the Bachelor of Science degree in particle physics from the Government Degree College for Boys, Baramulla, and the master's degree (Hons.) in electronics and instrumentation from the University of Kashmir, Hazratbal. In the master's degree, he has garnered recognition for his academic prowess. Previously, he was a Verification Engineer with Synopsys, Delhi, and currently conducts research with the Indian Institute of Technology Roorkee on an esteemed DST India Fellowship from the Government of India. His research interests include organic solar cell technology, silicon photonics, and VLSI design and verification, reflecting his diverse expertise. His academic journey has been marked by numerous accolades and scholarships, affirming his dedication to academic excellence.

FAISAL BASHIR (Member, IEEE) received the M.Sc. and M.Phil. degrees in electronic science from the University of Kashmir, Srinagar, India, and the Ph.D. degree in electronic science from Jami Millia Islamia, New Delhi, India. Besides this, he has qualified national eligibility test in electronic science for assistant professorship conducted by university grants commission. He is currently an Assistant Professor with the Department of Computer Engineering and CCS and IT, King Faisal University, Hofuf, Al Ahsa, Saudi Arabia. He has authored or coauthored more than 40 research publications and three book chapters in the field of semiconductor devices, neuromorphic computing, and VLSI design in reputed international journals and conferences. His research interests include neural networks semiconductor devices and modeling, VLSI design, and nano-electronics. He was a recipient of Best Paper Award in World Congress on Engineering held at Honk Kong 2014 and Merit Scholarship at M.Phil. Level from the University of Kashmir.

FAROOQ AHMAD KHANDAY (Senior Member, IEEE) received the B.Sc., M.Sc., M.Phil., and Ph.D. degrees from the University of Kashmir, in 2001, 2004, 2010, and 2013, respectively. From June 2005 to January 2009, he was an Assistant Professor on contractual basis with the Department of Electronics and Instrumentation Technology, University of Kashmir. In 2009, he joined the Department of Higher Education Jammu and Kashmir and the Department of Electronics and Vocational Studies, Islamia College of Science and Commerce, Srinagar, as an Assistant Professor. Since May 2010, he has been an Assistant Professor with the Department of Electronics and Instrumentation Technology, University of Kashmir. He is the author or coauthor of more than 80 publications in peer-reviewed indexed international and national journals/conferences of repute and three book chapters. His research interests include low-voltage analog integrated circuit design, fractional-order systems, hardware neural networks, biomedical circuit design, spintronics and nano-electronics, and stochastic computing.

FURQAN ZAHOOR (Member, IEEE) received the B.Tech. degree in electronics and communication engineering from the University of Kashmir, Srinagar, in 2014, the M.Tech. degree in electronics and communication engineering from Shri Mata Vaishno Devi University, Katra, in 2016, and the Ph.D. degree in electrical and electronics engineering from Universiti Teknologi PETRONAS, Malaysia, in 2022. From May 2017 to September 2018, he was an Assistant Professor on contractual basis with the Department of Electronics and Instrumentation Technology, University of Kashmir. He was a Postdoctoral Research Fellow with the School of Computer Science and Engineering, Nanyang Technological University, Singapore, from July 2022 to August 2023. He is currently a Postdoctoral Research Fellow with the Interdisciplinary Research Center for Advanced Materials, King Fahd University of Petroleum and Minerals, Saudi Arabia. His research interests include multiple valued logic (MVL), resistive random access memory (RRAM) devices, hardware security primitives, neuromorphic computing, and solar cells.

MEHWISH HANIF received the bachelor's degree in electronics from the COMSATS University of Science and Technology, Pakistan, in 2013, the Master of Philosophy degree in physics from Riphah International University, Pakistan, in 2016, and the Ph.D. degree in electrical and electronics engineering from Universiti Teknologi PETRONAS (UTP), Malaysia, in 2023. She is currently working at Tyndall National Institute, University College Cork, as a Postdoctoral Researcher. Her research interests include quantum electronic devices, acousto-optic devices, surface acoustic waves (SAW) sensors based on single and multilayer structure, investigation into the behaviors of different piezoelectric materials for SAW sensors, and nanomaterials'-based sensors.

ZAZILAH MAY (Graduate Student Member, IEEE) received the bachelor's degree in mathematics from the University of Leicester, U.K., in 1998, and the master's degree in advanced control from UMIST, U.K., in 2000. She is currently pursuing the Ph.D. degree in electrical, electronic and systems engineering from The National University of Malaysia. She is working is a Lecturer with the Department of Electrical and Electronic Engineering, Universiti Teknologi PETRONAS (UTP), Malaysia. She has more than 20 years of professional experiences in teaching and research. Her research interests include wireless communication, control systems, artificial intelligence, signal processing, and image processing. She involved in various projects related to oil and gas structural health monitoring.